


Increasing the corrosion resistance of the center plate unit in railway freight car

Maryna Bulakh^{1*} , Jarosław Bieniaś², Monika Ostapiuk², Dmytro Molchanov³, Olegas Lunys⁴, Leonty Muradian³

¹ Faculty of Mechanics and Technology, Rzeszow University of Technology, ul. Kwiatkowskiego 4, 37-450 Stalowa Wola, Poland

² Faculty of Mechanical Engineering, Lublin University of Technology, ul. Nadbystrzycka 36, 20-618 Lublin, Poland

³ Faculty of Transport Engineering, Ukrainian State University of Science and Technologies, Lazaryan Street, 2, Dnipro, 49010, Ukraine

⁴ Vilnius Gediminas Technical University, Saulėtekio al. 11, LT-10223 Vilnius, Lithuania

* Corresponding author's e-mail: m.bulakh@prz.edu.pl

ABSTRACT

One of the most damage-prone components of a freight car is the center plate, which is highly susceptible to wear and corrosion. This study investigated the application of a composite coating based on a FeCrNi alloy with the addition of chromium carbide (Cr_3C_2) to protect the steel surfaces of the center plate from corrosion and mechanical degradation. The coating was applied using laser cladding and subjected to comprehensive testing, including electrochemical analysis (OCP, polarization, and electrochemical impedance spectroscopy), microhardness measurements, and microstructure evaluation using scanning electron microscopy (SEM). The results showed that the coating exhibited a stable corrosion potential, low corrosion current density, and high impedance at low frequencies, indicating good protection against ion penetration and electrode reactivity, while significantly improving the microhardness of the base material. This study demonstrates the potential of the modified FeCrNi-based coating in extending the service life, enhancing the operational reliability, and increasing the corrosion resistance of center plates in freight cars.

Keywords: corrosion resistance, composite coating, microstructure and electrochemical properties, center plate unit, railway freight car, corrosion rate.

INTRODUCTION

Rail transport constitutes a key element of transportation infrastructure, playing a vital role in the socio-economic development of a country. It is characterized by high capacity, energy efficiency, and the ability to operate in diverse climatic conditions, which gives it an advantage over other modes of transport [1, 2].

Railways serve as a fundamental logistical link, supporting the operations of strategic sectors of the economy such as heavy industry, energy, and agriculture [3, 4]. The significant volume of freight transported, along with high demands for punctuality and safety, necessitates maintaining a

high level of technical efficiency in rolling stock. The technical condition of railcars, particularly the integrity and reliability of their structural components, has a direct impact on transport efficiency. Under typical railway operating conditions – including dynamic loads, vibrations, temperature fluctuations, and exposure to moisture and corrosive substances – many components undergo accelerated wear. This leads to increased operating costs, a higher risk of failures, and a reduced level of safety [5, 6]. A particularly damage-prone component is the center plate unit, which is responsible for transferring vertical loads from the car body to the bogie and allows the bogie to rotate relative to the body while negotiating curves.

This element is subjected to intense cyclic mechanical loads as well as environmental factors, which contribute to its wear and corrosion. An additional issue is the limited accessibility of the center plate unit, making inspection, lubrication, and replacement difficult. As a result, it represents a critical point in the wagon's structure, and its degradation can lead to serious hazards, including derailments and structural damage. The effects of prolonged exposure to adverse operating conditions can be clearly observed in real-world examples. Figure 1 shows a typical case of combined mechanical and corrosive wear observed in the center plate unit of a freight car after covering 140,000 kilometers.

In light of the aforementioned challenges, increasing the corrosion and wear resistance of the center bowl assembly is a current direction of research. Improving the protective properties of this component can significantly enhance the reliability and safety of freight rail transport, reduce maintenance costs and frequency, and extend the service life of freight cars. This directly translates into improved efficiency and stability of the entire railway sector.

Due to the central role of the center bowl assembly in the structure of freight cars [7], numerous efforts are being undertaken to extend its service life. These strategies vary depending on the predominant damage mechanisms. In many studies, friction in the contact zones is identified as the main cause of wear. In response, technological solutions are proposed to reduce it – such as the use of lubricants [8] and polymer liners [9–11] with varying physical and mechanical properties.

Innovative engineering solutions aimed at modernizing the center plate are presented in

[12, 13]. The primary goal of these approaches is to reduce wear intensity. In [12], a design is presented that allows for assembly without welding, enabling reduced maintenance time, lower operating costs, and the elimination of thermal stresses. Meanwhile, the studies described in [13] focus on optimizing the shape of the center plate by ensuring continuous contact with the cooperating side surfaces. This solution allows for more uniform load distribution, reduces edge contact, and eliminates horizontal plane clearance, resulting in reduced contact stresses, improved body stability, and increased operational durability of the component.

In addition to abrasive wear, corrosion has a significant impact on the degradation of center plate assemblies [14]. Due to their structural characteristics and operating conditions, these components are particularly susceptible to the effects of corrosive environments [15]. Corrosion not only leads to the loss of mechanical properties but also contributes to operational damage and maintenance issues [16].

Research on corrosion mechanisms is highly dependent on the type of material. While the corrosion behavior of high-alloy [17, 18] and low-carbon steels [19–21] has been analyzed under laboratory conditions, the construction of freight cars predominantly uses low-alloy structural steels, such as S235JR, S235JRG2, and S355JR according to EN 10025-2, which are functionally equivalent to the previously used 20GL, 20FL, and 20GFL under GOST standards. Their anticorrosive properties have been described in numerous studies [22–26], identifying grades with enhanced corrosion protection. However, due to structural limitations of the center plate

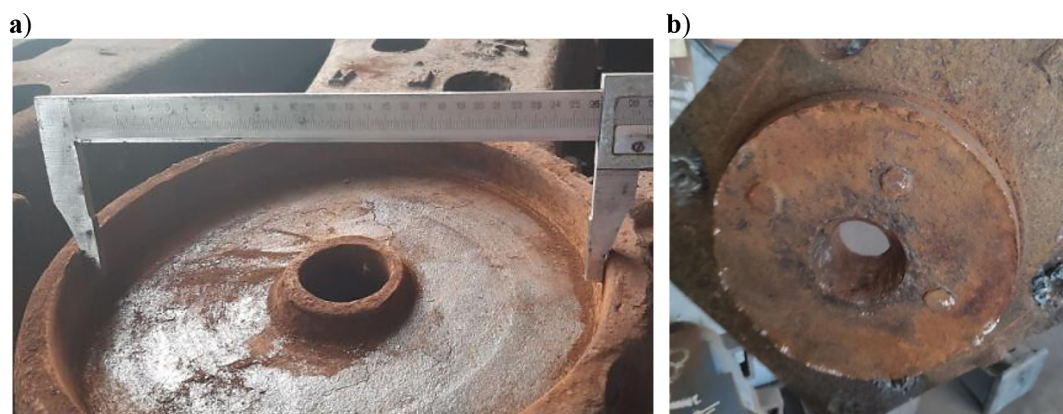


Figure 1. Example of mechanical and corrosion wear of the center plate unit of a freight car after 140,000 km in operation: (a) central bowl; (b) center plate

assembly, replacing the base material is often impractical. A more feasible approach is the use of protective coatings. Among the most promising methods are coatings made from metal powders [27, 28], various metal-ceramic coatings based on WC [29], microplasma spraying of coatings from heat-resistant nickel wire with laser melting [30], graphene-enhanced composites [31], and hybrid systems based on alkyd paints with the addition of 5 wt.% polyaniline [32, 33]. It is worth noting, however, that most of these methods focus primarily on corrosion protection or improving mechanical properties.

Due to the specific operating conditions in which the central plate assembly of a freight car operates, there is a clear need to develop engineering solutions that simultaneously ensure high corrosion resistance and increased operational durability. The complex geometry of this component promotes the accumulation of corrosion products, which leads to accelerated abrasive wear.

The aim of this study was to enhance the corrosion resistance of the central plate assembly by applying an advanced composite coating based on an iron-chromium-nickel (FeCrNi) alloy, enriched with 3 wt.% chromium carbide (Cr_3C_2). The coating was deposited onto a steel substrate using laser cladding technology.

The objective of the research is to characterize the microstructure and electrochemical properties of the coating, with particular emphasis on corrosion potential, corrosion current density, and impedance resistance under simulated atmospheric conditions and high humidity, typical of railway operation.

It is assumed that the implementation of coatings with optimized functional properties will significantly reduce the corrosion rate, increase mechanical resistance, and extend the service life of central plate assemblies, while also reducing the frequency of unplanned maintenance downtimes. The research findings may serve as a foundation for the implementation of innovative material solutions in the design and maintenance of freight rolling stock, with particular emphasis on the modernization of key load-bearing components.

The novelty of this work lies in the use of laser cladding technology to produce functional composite coatings based on FeCrNi with the addition of Cr_3C_2 , specifically adapted to the dynamic loading and environmental exposure conditions characteristic of railway operation. Importantly, the application of advanced impedance

analysis and equivalent circuit modeling enabled an in-depth understanding of the coating's barrier properties and the stability of the passive layer. The methodology employed integrates modern materials engineering with the practical requirements of railway infrastructure, offering a new paradigm in the design of multifunctional, durable protective coatings for structural components subjected to extreme operational loads.

MATERIALS AND METHODS

In response to the identified operational challenges, a composite protective coating was developed using commercially available metallic powders with a purity above 99.0%. The metallic matrix is composed of an iron-chromium-nickel powder, selected due to the synergistic combination of the beneficial properties of its constituents. Iron provides adequate mechanical strength and good machinability, chromium contributes to corrosion resistance by promoting the formation of a protective Cr_2O_3 oxide layer on the surface, while nickel stabilizes the alloy structure, reduces residual stresses generated during the cladding process, and improves the adhesion of the coating to the steel substrate.

To enhance the coating's stability to mechanical wear, 3 wt.% of Cr_3C_2 particles were added to its composition. The reinforcing particles were uniformly dispersed throughout the metallic matrix, contributing to the formation of a homogeneous microstructure with low porosity. This morphology reduces the risk of crack initiation and the occurrence of local defects that could compromise the mechanical integrity of the coating. The chemical composition of the coating is given in Table 1. The chemical composition presented in Table 1 refers to the nominal composition of the feedstock powder mixture, which was prepared prior to laser cladding using commercially available metallic powders with a purity exceeding 99.0%.

The individual elemental percentages (Fe – 59%, Cr – 8%, Ni – 30%, Cr_3C_2 – 3%) were determined based on:

- manufacturer specifications for each powder (provided in the material certificates);
- controlled weighing and blending of the powders in precise proportions using a powder feeder system calibrated by mass flow rate.

Table 1. Composition of composite coating

Fe, %	Cr, %	Ni, %	Cr ₃ C ₂ , %
59.0	8.0	30.0	3.0

Although the final composition of the coating was not measured directly after cladding via, the homogeneous microstructure and uniform distribution of phases indicate that the chemical integrity of the blend was preserved during deposition.

The composite coating was obtained through single-layer deposition of a powder mixture onto the surface of steel substrates using laser cladding technology. The process was carried out with the use of a robotic laser system, TruLaser Robot 5020 (Trumpf).

The following parameters were applied: laser power – 2.0 kW; head traverse speed – 240 mm/min; powder feed rate – 4.5 rpm; transport gas flow rate – 6 l/min; shielding gas flow rate – 16 l/min. The final thickness of the coatings did not exceed 4 mm, which allowed for achieving a layer with suitable functional characteristics without adverse effects of excessive substrate heating.

For corrosion resistance testing, samples with dimensions of 15 × 15 × 4 mm were prepared, ensuring an adequate surface area for uniform exposure to the corrosive environment. After cutting, the samples underwent preparatory treatment involving sequential grinding with abrasive papers of grit sizes ranging from P320 to P2000, followed by polishing using diamond suspensions until a mirror-like surface finish was achieved. The cutting process was performed on a Struers Secotom-10 precision cutter, which minimized the thermal impact on the material's microstructure and preserved its original morphological features for further analysis.

To evaluate microhardness, smaller samples (5 × 5 × 5 mm) were prepared to allow for localized measurements. To facilitate subsequent preparation stages and to protect the edges of the samples from mechanical damage, the specimens were embedded in a cold-curing polymer resin. These prepared samples were mounted in cylindrical molds, providing stable support during further grinding and enabling the formation of a uniform, homogeneous analytical surface.

The applied sample preparation methods enabled the achievement of high-quality test surfaces, allowing for precise assessment of corrosion and mechanical properties essential for the comprehensive characterization of the coatings

produced by laser deposition. To assess the corrosion properties of the tested coatings, a series of electrochemical tests were conducted, including open circuit potential (OCP) measurements, potentiodynamic polarization curves, and electrochemical impedance spectroscopy (EIS). The analyses were performed in a synthetic corrosive environment, i.e., an aqueous solution of 3.5 wt.% NaCl, at room temperature. The experiments were carried out using an Atlas 0531 potentiostat (Atlas-Sollich, Poland), equipped with a frequency response analysis (FRA) module.

A standard three-electrode setup was used for the tests, in which a saturated calomel electrode served as the reference electrode, a platinum foil was used as the counter electrode, and the tested coating was used as the working electrode. The active surface area of the sample was limited to 1 cm². During the recording of potentiodynamic polarization curves, the sample was polarized in the frequency range from 100 kHz to 0.01 Hz relative to the open circuit potential, with a scan rate of 1 mV/s. The amplitude of the sinusoidal signal was 10 mV. The obtained impedance spectra were presented in the form of Bode and Nyquist plots, which allowed for a comprehensive analysis of the electrochemical characteristics of the coatings.

To study the changes in the macro- and microstructure of the samples before and after exposure to the corrosive environment, a stereoscopic microscope (model NIKON SMZ 1500, manufactured by Nikon, Tokyo, Japan) and a scanning electron microscope (SEM, NovaNanoSEM 450, FEI Company Japan Ltd., Tokyo, Japan) were used. SEM studies were carried out in low vacuum mode at a pressure of 100 Pa at acceleration voltages of 10 and 15 keV.

In order to assess the influence of the content of powder components on the mechanical properties of composite coatings, microhardness measurements of the manufactured samples were carried out. The tests were performed according to the ISO 6507-4:2018 standard [34] using the Vickers HV0.3 method at a load of 2.94 N. The microhardness parameters were determined by the sizes of the indenter indentation diagonals.

The surfaces of the samples were cleaned and prepared with special care before testing in order to eliminate the influence of possible contamination on the accuracy of the results. The measurements were carried out using a microhardness tester model QNESS 10/60 M manufactured by

ATM Qness GmbH (Mammelzen, Germany). This device provides a high level of accuracy due to stable control of the applied load and reliability of the measurement process.

Five measurements were performed on each sample at different points on the surface, which allows taking into account the heterogeneity in the distribution of microhardness over the coating plane. For each sample, the arithmetic mean of the three most representative values was calculated, which eliminates the influence of single anomalies.

RESULTS AND DISCUSSION

Corrosion tests

Results of the open circle potential (OCP) study

During the study, an analysis of the values of the open corrosion potential was conducted for coating samples, each of which was characterized by its own time interval of stabilization. The studies allowed us to quantitatively evaluate the anticorrosive efficiency of the coating. The calculation was performed within ± 100 points around the characteristic moment of stabilization. The calculation results are presented in Figure 2.

The electrochemical stability of the analyzed coating was further confirmed through a statistical analysis of the OCP over time. The time required to reach a relative potential stabilization phase, approximately 304 seconds, indicates rapid

stabilization of the electrode–electrolyte system, which is important for the effective formation of a coating on the material surface. The average OCP value, determined to be -0.449 V, suggests a relatively passive character of the surface following the initial period of corrosive activity. However, because the time axis in Figure 2 is presented on a linear scale, the dynamics of this stabilization process are not easily discernible. A logarithmic time scale would better illustrate the slowdown in potential change, allowing clearer identification of the quasi-steady-state region.

The standard deviation of the recorded signal, amounting to 0.063 V, indicates a low level of potential fluctuations over time, which can be interpreted as evidence of a stable electrochemical state of the material in the examined corrosive environment. This small deviation of the OCP values from the average confirms the uniformity of surface reactions as well as good adhesion and coherence of the protective coating, which translates into a reduction of local corrosion cells and increased stability of the system to electrochemical degradation.

Results of potentiodynamic polarization

To assess the electrochemical activity of the tested coating, a potentiodynamic polarization test was conducted. Figure 3 presents the obtained Tafel curves, from which the main electrochemical parameters were determined: the corrosion potential (E_{corr}) and the corrosion current density

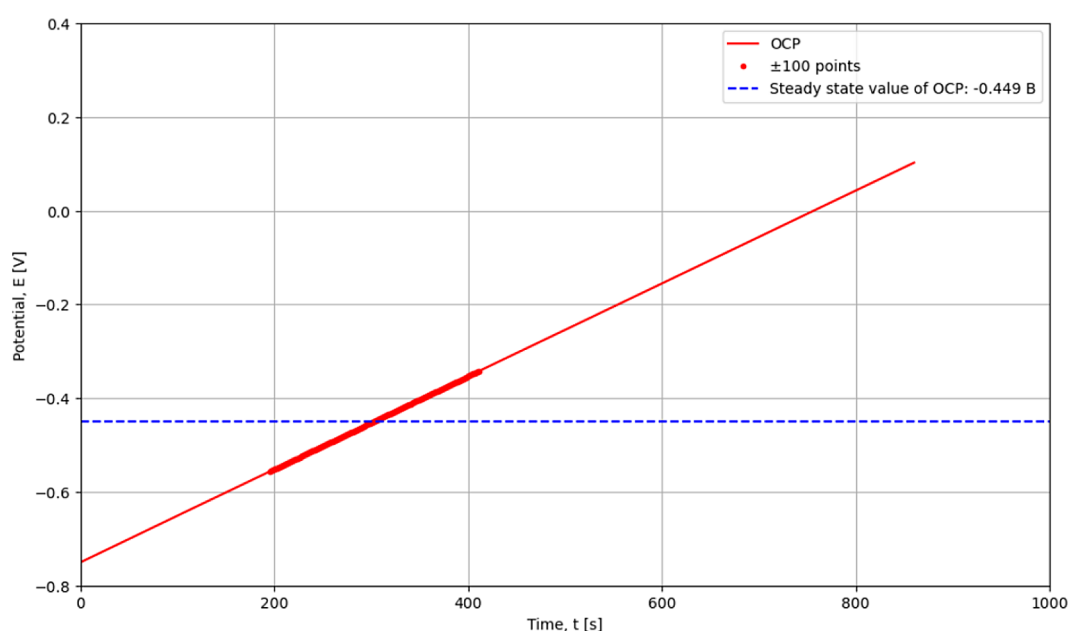


Figure 2. Open corrosion potential of composite coating

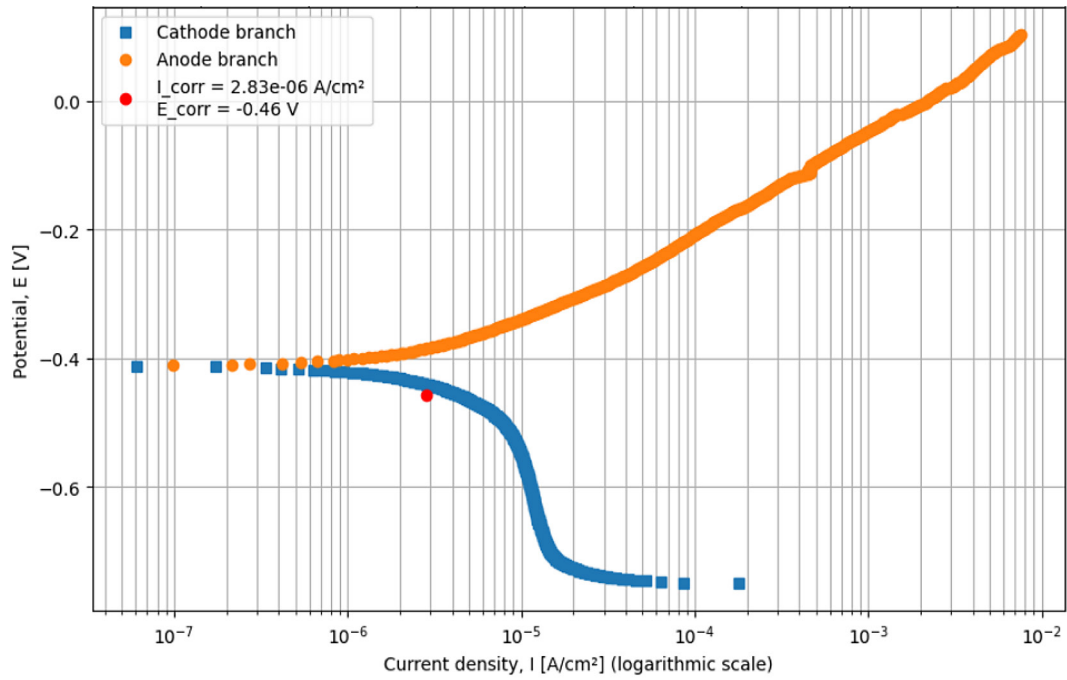


Figure 3. Tafel curves

(i_{corr}). These indicators are quantitative measures of the material's stability to corrosion degradation.

The polarization curve clearly shows well-defined anodic (orange points) and cathodic (blue points) branches, which allows for the determination of key electrochemical parameters such as the corrosion potential (E_{corr}) and corrosion current density (I_{corr}). Based on the intersection of the extrapolated linear portions of both branches, the following values were determined: $E_{\text{corr}} = -0.46$ V and $I_{\text{corr}} = 2.83 \times 10^{-6}$ A/cm².

The corrosion potential value indicates the tendency of the tested material to corrode in the given environment. The negative E_{corr} value suggests a relatively high thermodynamic tendency for oxidation. On the other hand, the low

corrosion current density indicates good corrosion resistance of the material, which may result from surface passivation or the effective performance of a protective coating.

Results of electrochemical impedance spectroscopy

To evaluate the anti-corrosion properties of the composite coating, a Bode curve was constructed using electrochemical impedance spectroscopy (EIS). The results are presented in Figure 4.

The impedance modulus $|Z|$ decreases with increasing frequency (Figure 4(a)). Such behavior is typical of capacitive or diffusion-controlled systems. This indicates partially effective

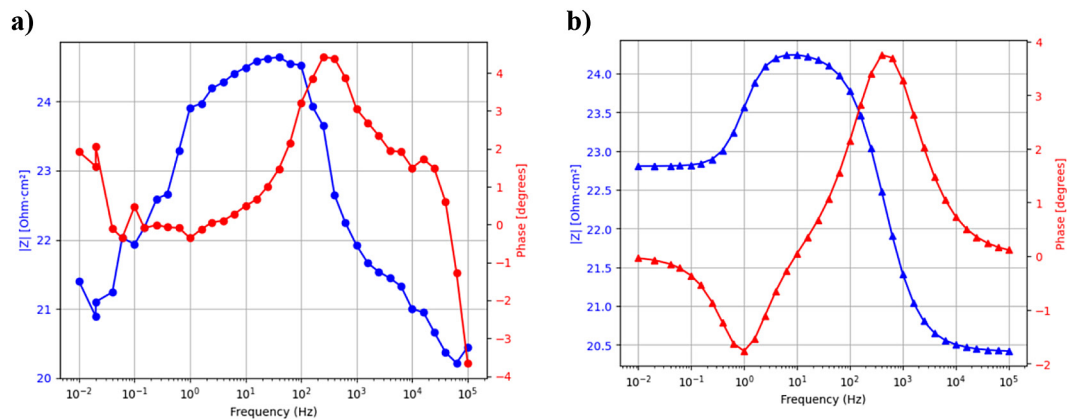


Figure 4. Bode curves: (a) experimental results; (b) model

passivation. The Bode plot shows that the addition of Cr_3C_2 enhances passivation and reduces surface reactivity, but makes it more heterogeneous, reinforcing capacitive-diffusive processes. Figure 4b shows that the selected model effectively replicates the observed drop in impedance and phase behavior. In the mid-frequency range, a phase shift and a resistance maximum are observed due to inductance and the additional resistances R_1/R_2 . The CPE parameters allow for an accurate description of non-ideal capacitive processes (surface roughness, porosity, etc.). The CPE exponent n is less than 1. The proposed model appropriately describes all the characteristic segments of the experimental curves, including the influence of inductance, diffusion, and surface effects, and can be recommended for analyzing similar systems. As evidence of the above, the RMS error for the absolute value of $|Z|$ is approximately $0.642 \text{ Ohm}\cdot\text{cm}^2$, and the RMS phase error is approximately 1.17° . This confirms the high accuracy of the models. The model and its parameters will be presented below.

A reference EIS measurement on the uncoated substrate material was not performed in the current work. Future studies will include comparative electrochemical impedance analysis to quantify the improvement in charge transfer stability, coating capacitance, and barrier properties relative to the base steel. Figure 5 shows the impedance spectra (Nyquist plots) for the tested

coating, demonstrating a similar general morphology characteristic of a typical Randles-type equivalent electrical circuit.

The curves are semicircular in shape, indicating the dominance of charge transfer stability and double-layer capacitance in the investigated systems. Due to visible deviations and low-frequency distortion, precise numerical fitting should be interpreted with caution (Figure 5). Additional repetitions and averaging will be performed in follow-up experiments to improve spectral clarity and reproducibility.

The experimental curve exhibits an irregular semicircular shape, with clear disturbances and instabilities in the mid-frequency range. The initial increase in $-\text{Im}(Z)$ at low frequencies indicates the dominant influence of capacitive elements (such as the double layer and passivation effects). The flattening of the curve in the central part suggests the presence of additional relaxation processes, such as ion diffusion or adsorption. The presence of a second arc or deviation may indicate an additional electrochemical process, e.g., a secondary reaction or the influence of a porous surface structure.

The lower end of the curve approaching the real axis ($\text{Re}(Z)$) indicates a reduced influence of reactive components at high frequencies and the dominance of electrode stability.

The theoretical model (red line) reflects the general trend of the experimental curve,

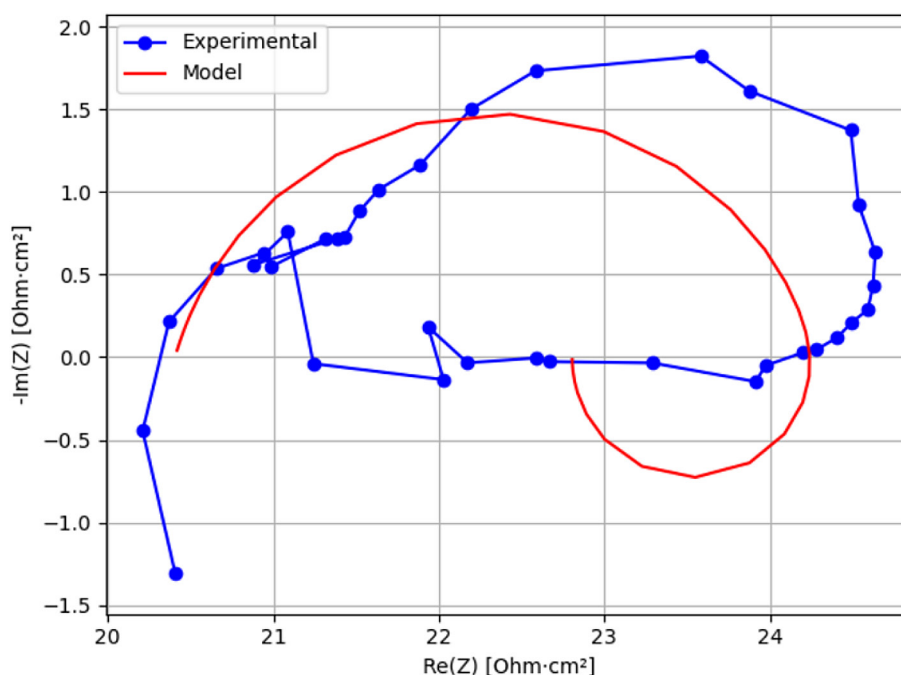


Figure 5. Nyquist curves

especially in the high- and mid-frequency range, but shows some discrepancies at low frequencies and in the shape of the lower arc. This may result from simplifications in the model or from system non-stationarity (e.g., local degradation, micro-reactions in the coating). Nevertheless, the model accounts for the main processes occurring at the phase boundary and allows for the extraction of significant electrochemical parameters.

A reference Nyquist measurement of the uncoated steel substrate is not included in the present study. Future work will incorporate side-by-side EIS analysis to quantitatively assess the protective effect of the FeCrNi–Cr₃C₂ coating relative to base material impedance parameters.

The model results presented in Figures 4 and 5 were obtained based on the same equivalent circuit, which is shown in Figure 6. The high-frequency part of the spectra demonstrates similar R_s values, indicating consistent electrolyte conductivity across all measurements.

The model parameters for the equivalent circuit (Figure 6) are given in Table 2.

The selected parameters of the equivalent circuit model, presented in Table 2, were used to construct the curves shown in Figures 4 and 5.

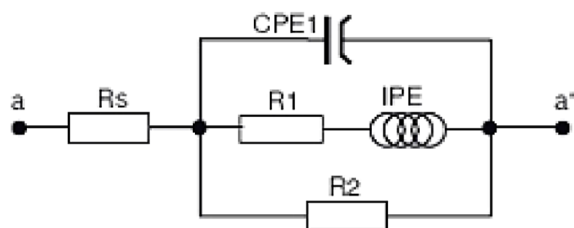


Table 2. Model parameters for the equivalent circuit

Parameter	Fitted parameter (with Units)
R_s	18.74 $\Omega \cdot \text{cm}^2$
R_1	4.25 $\Omega \cdot \text{cm}^2$
L	0.324 H
R_2	4.17 $\Omega \cdot \text{cm}^2$
CPE Y	0.000273 S/ cm^2

The obtained modeling results are in good agreement with the experimental data.

Corrosion rate

The value of corrosion rate V in mm/year is calculated as:

$$V = \frac{0.00327 \times J_{\text{corr}} \times EW}{\rho} \quad (1)$$

where: 0.00327 is a constant (to convert units); J_{corr} is corrosion current density, $\mu\text{A}/\text{cm}^2$; EW is equivalent weight, g/equiv, ρ is alloy density, g/cm^3 .

The results are presented in Table 3, which now includes reference values from literature for uncoated low-alloy steels (e.g., S235JR or 20GL equivalents) under similar test conditions (3.5% NaCl solution). The corrosion rate of the composite coating is nearly ten orders of magnitude lower than that of uncoated structural steels exposed to identical chloride-rich environments. This confirms that the FeCrNi–Cr₃C₂ system effectively suppresses electrochemical degradation, primarily through the formation of a passive Cr₂O₃-rich surface and the structural stability imparted by Cr₃C₂ ceramic reinforcement.

The test results confirm the potential use of Cr₃C₂ in Fe-Ni-Cr alloys where increased mechanical or wear stability is desired without compromising electrochemical stability. These findings reinforce the suitability of this coating for protecting critical railway components from long-term corrosion in harsh operational conditions.

Microhardness tests

The results of measuring the average microhardness of the studied coatings are shown in Figure 7. The results of the average microhardness measurements of the tested coatings indicate a significant influence of Cr₃C₂ content on the coating's microhardness. The addition of carbide to the coating leads to a noticeable improvement in mechanical properties.

The coating exhibits significantly higher microhardness, ranging from 390 to 420 HV. This means it is nearly twice as hard as all three

Table 3. Corrosion rate comparison between coated and uncoated materials

Sample	I_{corr} , $\mu\text{A}/\text{cm}^2$	EW, g/equiv	ρ , g/cm^3	Corrosion rate, mm/year
FeCrNi–Cr ₃ C ₂ coating	2.83×10^{-3}	61.4	7.9	7.20×10^{-5}
Uncoated steel	$20\text{--}30 \times 10^{-3}$	~56–60	~7.8	$\sim 4.7\text{--}7.6 \times 10^{-4}$

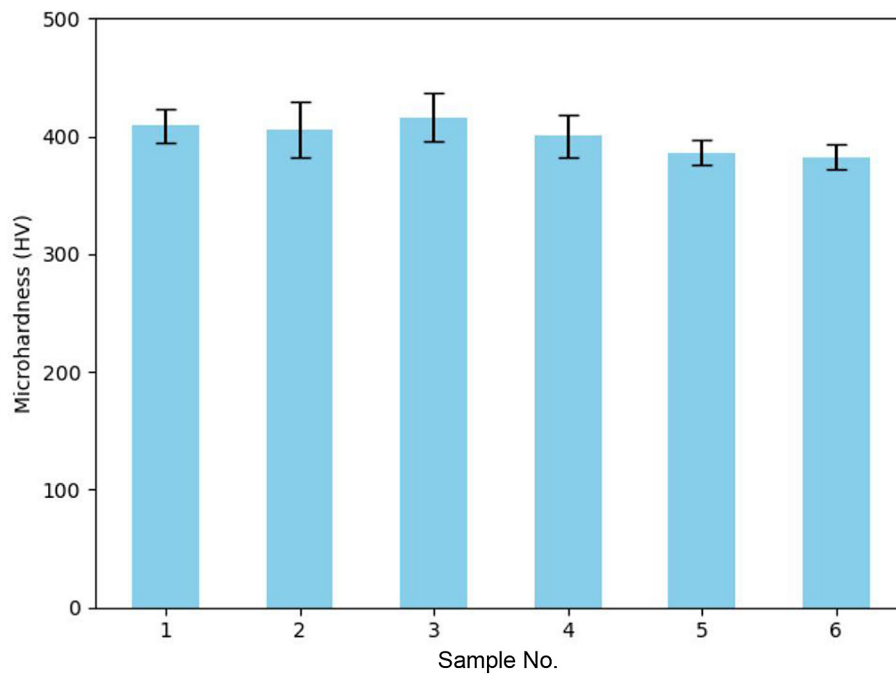


Figure 7. Results of measuring the average microhardness of the studied coatings

compared steel grades (20GL, 20FL, 20GFL – 140–220 HV). Such high hardness indicates effective structural strengthening of the material, which may result from the presence of ceramic phases such as Cr_3C_2 or from the dispersion of hard reinforcing particles within the coating matrix. High hardness also suggests substantially greater stability to plastic deformation, wear, and micro-damage, making the coating particularly suitable for mechanically demanding applications.

SEM analysis results

The SEM analysis results presents cross-sectional high-resolution images (Figure 8, a) and EDS elemental maps (Figure 8, b) to evaluate the micro-structure and composition of the coated surface.

This backscattered electron image (Figure 8, a) shows a cross-sectional view of the FeCrNi– Cr_3C_2 coating. The image reveals a dense and uniform layer with good adhesion to the steel substrate.

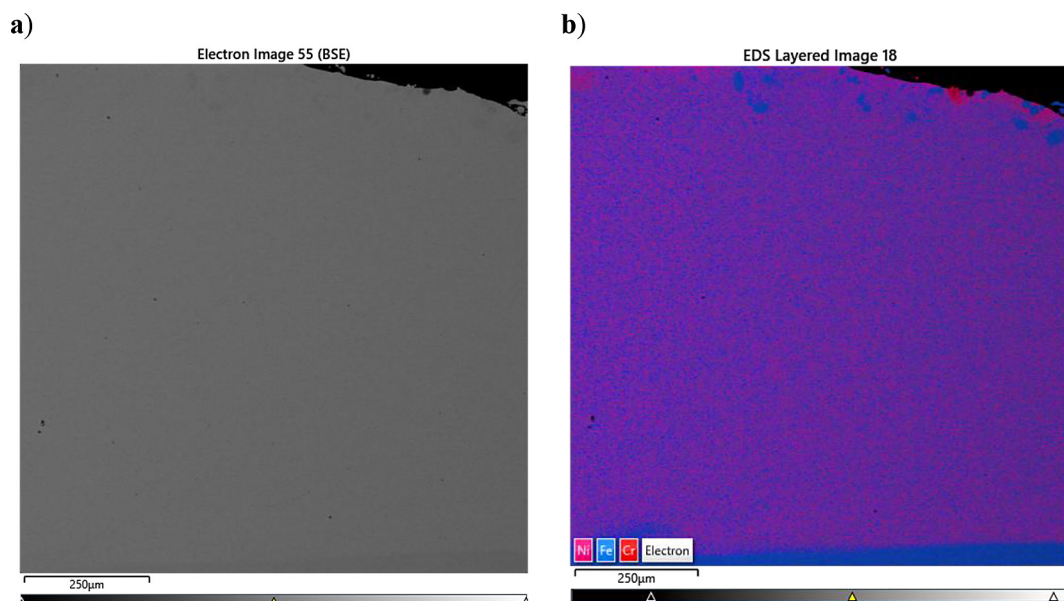


Figure 8. Electron image (BSE mode) (a); EDS layered image (b)

Bright regions correspond to metallic matrix phases, while dark, irregularly shaped inclusions represent ceramic Cr_3C_2 particles.

No significant porosity or cracking is visible, confirming process stability. The composite EDS layered image (Figure 8, b) presents an overlay of Fe, Cr, and Ni elemental distributions across the cross-section. A homogeneous distribution of alloying elements is evident. Iron is mainly concentrated in the matrix and the steel substrate. Its uniform distribution confirms the dominance of Fe in the bulk and clad layers. Areas with lower Fe content correspond to Cr_3C_2 inclusions. Chromium shows strong presence throughout the coating, particularly around carbide particles.

Nickel is uniformly distributed in the matrix, contributing to solid-solution strengthening. Ni enhances the structural integrity of the coating and improves adhesion. Its consistency supports metallurgical bonding without phase separation.

Figure 9 shows the microstructures of the coating in SEM analysis after corrosion attack. This allowed us to identify differences in the morphology and extent of corrosion damage.

The SEM image of the coating reveals a complex, clearly heterogeneous microstructure, indicative of the multiphase nature of the material. Numerous dark inclusions with irregular shapes and varying sizes are distributed across the entire surface. The black inclusions observed in the SEM images after exposure to the corrosive environment are interpreted as localized corrosion products, likely composed of iron and chromium oxides or

hydroxides that have formed in micro-defect regions of the coating surface. The gray regions represent the FeCrNi metallic matrix, which remains mostly intact due to its passivation properties. This distinction is important to highlight zones of localized electrochemical degradation, which provide insight into the coating's corrosion behavior.

The lower-magnification image (Figure 9a) shows the general surface condition and distribution of corrosion-affected zones. The higher-magnification image (Figure 9b) allows a closer examination of corrosion morphology, including the interaction between corroded areas and the surrounding matrix. Together, these images illustrate the localized nature of corrosion, the effectiveness of the coating in limiting its spread, and the structural integrity of the matrix.

These inclusions most likely correspond to Cr_3C_2 , intentionally added to enhance the mechanical strength of the coating through dispersion strengthening. Their irregular yet well-integrated morphology suggests an effective anchoring mechanism within the matrix, which positively influences wear and microcrack protection.

Distinct dendritic structures or crystallization texture patterns are visible between the matrix areas and the inclusions, which may result from rapid cooling processes or differences in the thermal conductivity of the phases. Such morphology promotes increased mechanical stiffness and may indicate a gradient microsegregation structure.

The microstructure of the coating demonstrates a high quality of dispersion strengthening, which

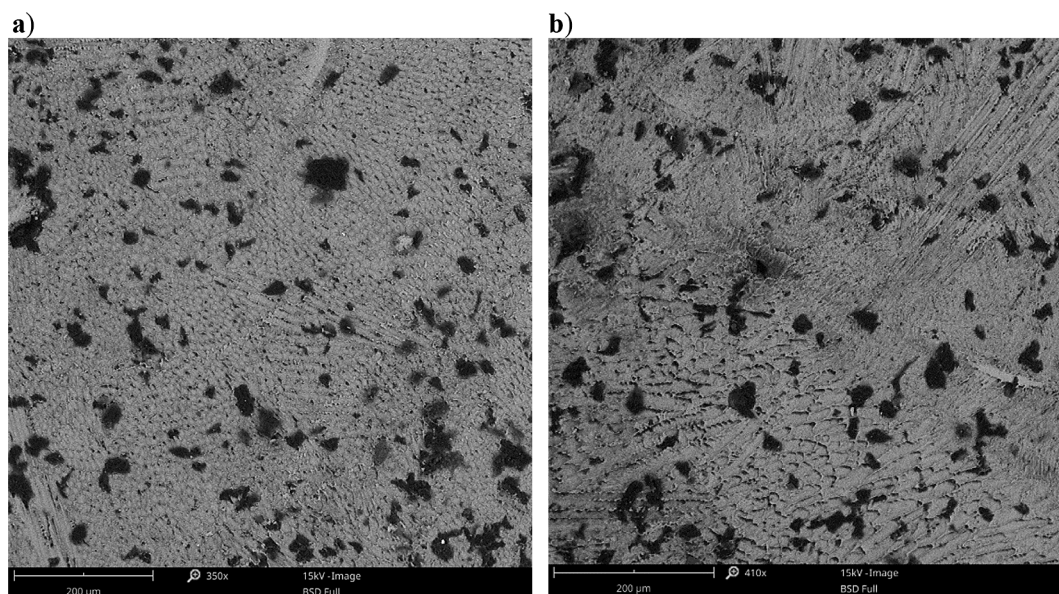


Figure 9. SEM analysis of the surface of the coating after corrosion: (a) 350x; (b) 410x

translates into excellent mechanical stability and potential durability under tribological conditions.

The presence of numerous hard particles, evenly distributed within the matrix, suggests an effective combination of structural and protective functions of the coating. The complex microstructure may be advantageous in applications with high mechanical demands, such as components of freight cars operating under heavy loads and in corrosive-abrasive environments.

CONCLUSIONS

This study presents the results of research on the application of a composite coating based on a FeCrNi alloy with the addition of 3 wt.% Cr₃C₂, aimed at enhancing the corrosion and mechanical stability of the center plate assembly in freight cars. The coating was applied using laser cladding technology with metallic powders, which enabled the formation of a dense layer with a uniform microstructure and low porosity. The coating was thoroughly characterized in terms of microstructure, microhardness, and electrochemical properties under simulated corrosive environment conditions.

Electrochemical analyses (OCP, potentiodynamic polarization, EIS) demonstrated that the developed coating exhibits a stable corrosion potential, low corrosion current density, and high impedance at low frequencies, indicating effective protection against ion penetration and electrode reactivity. The analysis of Nyquist plots confirmed that the system's behavior can be described using an extended Randles model, incorporating capacitive, diffusive, and inductive elements.

The microhardness of the coating reached values of 390–420 HV, representing a significant improvement compared to the base low-alloy steels (20GL, 20FL, 20GFL – 140–220 HV). SEM observations revealed the presence of hard Cr₃C₂ particles uniformly distributed within the FeCrNi matrix, contributing to improved stability to wear and microdamage.

However, several limitations of this work must be acknowledged:

- electrochemical testing was performed only on the coated sample; no reference measurements were taken on the uncoated substrate, limiting the ability to quantitatively evaluate the coating's relative performance;
- the OCP measurement duration was sufficient for observing early passivation trends but

may not fully reflect long-term stabilization behavior;

- some irregularities in the impedance data suggest the need for repeated trials and signal refinement to improve modeling accuracy.

In comparison to alternative coating technologies—such as graphene-enhanced polymer systems or alkyd-based composites with polyaniline (as discussed in the introduction)—the proposed metallic-ceramic coating provides superior mechanical performance, thermal stability, and structural integrity under dynamic loading conditions. While polymer-based coatings offer advantages like lightweight and easier application, their long-term wear behavior and load-bearing capacity are often insufficient for heavily loaded mechanical interfaces such as the center plate.

The application of the FeCrNi–Cr₃C₂ composite coating has the potential to significantly improve the corrosion resistance and mechanical properties of a critical component for the operational safety of freight cars. The research results indicate that the proposed solution may contribute to extending service life, reducing maintenance costs, and increasing the reliability of railway structures.

Acknowledgments

The research leading to these results has received funding from the commissioned task entitled “VIA CARPATIA Universities of Technology Network named after the President of the Republic of Poland Lech Kaczyński”, under the special purpose grant from the Minister of Science, contract no. MEiN/2022/DPI/2578 from October 26, 2022 action entitled “In the neighborhood - inter-university research internships and study visits.

REFERENCES

1. Jalolova M., Amirov L., Askarova M., Zakhidov G. Territorial features of railway transport control mechanisms. *Transp. Res. Proc.* 2022; 63: 2645–2652. <https://doi.org/10.1016/j.trpro.2022.06.305>
2. Baranovskyi D., Myamlin S., Podosonov D., Muradian L. Determination of the filler concentration of the composite material to reduce the wear of the central bowl of the rail truck bolster. *Ain Shams Eng. J.* 2023; 102232. <https://doi.org/10.1016/j.asej.2023.102232>

3. Pittman R., Jandová M., Król M., Nekrasenko L., Paleta T. The effectiveness of EC policies to move freight from road to rail: Evidence from CEE grain markets. *Res. Transp. Bus. Manag.* 2020; 37: 100482. <https://doi.org/10.1016/j.rtbm.2020.100482>
4. Lingaitis L.P., Mjamlin S., Baranovsky D., Jas-tremskas V. Prediction methodology of durability of locomotives diesel engines. *Ekspl. i Niezaw. – Mainten. and Reliab.* 2012; 14(2).
5. Baranovskyi D., Myamlin S. The criterion of development of processes of the self organization of subsystems of the second level in tribosystems of diesel engine. *Sci. Rep.* 2023; 13: 5736. <https://doi.org/10.1038/s41598-023-33015-3>
6. Baranovskyi D., Myamlin S., Kebal I. Increasing the carrying capacity of the solid-body rail freight car. *Adv. Sci. Technol. Res. J.* 2022; 16(3): 219–225. <https://doi.org/10.12913/22998624/149935>
7. Poveda-Reyes S., Rizzetto L., Triti C., Shi D., García-Jiménez E., Molero G. D., Santarremigia F. E. Risk evaluation of failures of the running gear with effects on rail infrastructure. *Eng Fail. Anal.* 2021; 128: 105613. <https://doi.org/10.1016/j.engfailanal.2021.105613>
8. Liu X., Wang Y., Qin L., Guo Z., Lu Z., Zhao X., Dong H., Xiao Q. Friction and wear properties of a novel interface of ordered microporous Ni-based coating combined with MoS₂ under complex working conditions. *Tribol. Int.* 2023; 189: 108970. <https://doi.org/10.1016/j.triboint.2023.108970>
9. Valente L., Lopes L., Ribeiro L.S. Influence of bogie maintenance and retrofitting on wheel wear: analysis using integer programming and multibody simulation. *Appl. Sci.* 2023; 13(10): 6101. <https://doi.org/10.3390/app13106101>
10. Wajih K. Improved combination wear and lubricating liner assembly for railway car truck bolster bowl. EP0654389B1. European Patent Office. 1999-09-29.
11. Opala M. Evaluation of bogie centre bowl friction models in the context of safety against derailment simulation predictions. *Arch. Appl. Mech.* 2018; 88: 943–953. <https://doi.org/10.1007/s00419-018-1351-4>
12. Wu H., Robeda J. Effects of bogie centre plate lubrication on vehicle curving and lateral stability. Dynamics of Vehicles on Roads and on Tracks. In: Proceedings of the 18th IAVSD Symposium Held in Kanagawa, Japan, August 24-30, 2003.
13. Swoboda A. L. Railway truck bolster center bowl liner. US20190106131A1. United States. 2020-05-19.
14. Olshevskiy A., Kim C. W., Yang H. I., Olshevskiy A. Wear simulation for the centre plate arrangement of a freight car. *Veh. Syst. Dyn.* 2015; 53(6): 856–876. <https://doi.org/10.1080/00423114.2015.1023319>
15. Koushik B. G., Van den Steen N., Mamme M. H., Van Ingelgem Y., Terryn H. Review on modelling of corrosion under droplet electrolyte for predicting atmospheric corrosion rate. *J. Mater. Sci. Technol.* 2021; 62: 254–267. <https://doi.org/10.1016/j.jmst.2020.04.061>
16. Wu H., Lei H., Chen Y. F., Qiao J. Comparison on corrosion behaviour and mechanical properties of structural steel exposed between urban industrial atmosphere and laboratory simulated environment. *Constr. Build. Mater.* 2019; 211: 228–243. <https://doi.org/10.1016/j.conbuildmat.2019.03.207>
17. Liu Y., Zhang J., Wei Y., Wang Z. Effect of different UV intensity on corrosion behavior of carbon steel exposed to simulated Nansha atmospheric environment. *Mater. Chem. Phys.* 2019; 237: 121855. <https://doi.org/10.1016/j.matchemphys.2019.121855>
18. Liu Z.Y., Hao W.K., Wu W., Luo H., Li X.G. Fundamental investigation of stress corrosion cracking of E690 steel in simulated marine thin electrolyte layer. *Corros. Sci.* 2019; 148: 388–396. <https://doi.org/10.1016/j.corsci.2018.12.029>
19. Ma H.C., Fan Y., Liu Z.Y., Du C.W., Li X.G. Effect of pre-strain on the electrochemical and stress corrosion cracking behavior of E690 steel in simulated marine atmosphere. *Ocean Eng.* 2019; 182: 188–195. <https://doi.org/10.1016/j.oceaneng.2019.04.044>
20. Iswanto P., Yaqin R.I., Akhyar i Sadida, H.M. Influence of shot peening on surface properties and corrosion resistance of implant material AISI 316L. *Metalurgija*, 2020; 59(3): 309–312. <https://hrcak.srce.hr/237025>
21. Iswanto P., Akhyar H., Faqihudin A. Effect of shot peening on microstructure, hardness, and corrosion resistance of AISI 316L. *Journal of Achievements in Materials and Manufacturing Engineering* 2018; 89(1): 19–26. <https://doi.org/10.5604/01.3001.0012.6668>
22. Wang Y., Mu X., Dong J., Umoh A. J., Ke W. Insight into atmospheric corrosion evolution of mild steel in a simulated coastal atmosphere. *J. Mater. Sci. Technol.* 2021; 76: 41–50. <https://doi.org/10.1016/j.jmst.2020.11.021>
23. Jia C., Shao Y., Guo L., Liu Y. Incipient corrosion behavior and mechanical properties of low-alloy steel in simulated industrial atmosphere. *Constr. Build. Mater.* 2018; 187: 1242–1252. <https://doi.org/10.1016/j.conbuildmat.2018.08.082>
24. Gao J.-W., Dai X., Zhu S.-P., Zhao J.-W., Correia J.A.F.O., Wang Q. Failure causes and hardening techniques of railway axles – A review from the perspective of structural integrity. *Eng Fail. Anal.* 2022; 141: 106656. <https://doi.org/10.1016/j.engfailanal.2022.106656>
25. Song J., Chen J., Yi P., Chen N., Li Z., Xiao K. Correlation between indoor and outdoor corrosion

- tests for coal train body steel in a coal medium environment. *J Iron Steel Res Int.* 2022; 29, 1495–1504. <https://doi.org/10.1007/s42243-022-00758-8>
26. He C., Yu W., Tang D. The effect of microstructure on the initial corrosion behavior of low carbon steel in simulated coal solution. *Mater. Res. Express* 2024; 11(5). <https://doi.org/10.1088/2053-1591/ad4cb9>
27. Klenam D. E. P., Chown L. H., Papo M. J., Cornish L. A. Steels for rail axles – an overview. *Crit. Rev. Solid State Mater. Sci.* 2022; 49(2): 163–193. <https://doi.org/10.1080/10408436.2022.2137462>
28. Huang J., Zhu Z., Wang H., Li K., Shi W., Jiao T. Effect of WC content on microstructure and properties of CoCrFeNi HEA composite coating on 316L surface via laser cladding. *Mater.* 2023; 16: 2706. <https://doi.org/10.3390/ma16072706>
29. Jonda E., Łatka L., Maciej A., Khozhanov A. Investigations on the microstructure and corrosion performance of different WC-based cermet coatings deposited by high velocity oxy fuel process onto magnesium alloy substrate. *Adv. Sci. Technol. Res. J.* 2023; 17(2): 25–35. <https://doi.org/10.12913/22998624/160513>
30. Korzhyk V, Gao S, Khaskin V, et al. Microplasma spraying of coatings from wire of heat-resistant nickel alloy Inconel 82 with laser melting. *Adv. Sci. Technol. Res. J.* 2025; 19(7): 164–178. <https://doi.org/10.12913/22998624/203733>
31. Meng X., Xiao S., Wu C., Li W., Fan S., Shi K., Chu P. K. Enhanced hydrogen resistance of X70 pipeline steels by adaptive growth of NiCr composite coatings with Cr/FexNi inlaid structures. *J. Alloys Compd.* 2024; 997: 174932. <https://doi.org/10.1016/j.jallcom.2024.174932>
32. Kumar S. S. A., Bashir S., Ramesh K., Ramesh S. New perspectives on Graphene/Graphene oxide based polymer nanocomposites for corrosion applications: The relevance of the Graphene/Polymer barrier coatings. *Prog. Org. Coat.* 2021; 154: 106215. <https://doi.org/10.1016/j.porgcoat.2021.106215>
33. Grgur B.N., Popović A.S., Salem A. Influence of alkyd composite coatings with polyaniline doped with different organic acids on the corrosion of mild steel. *Metals* 2023; 13(8): 1364. <https://doi.org/10.3390/met13081364>
34. ISO 6507-4:2018; Metallic Materials – Vickers Hardness Test – Part 4: Tables of Hardness Values. ISO Copyright Office: Geneva, Switzerland, 2018.